Asian Journal of Chemistry; Vol. 35, No. 10 (2023), 2481-2486

ASIAN JOURNAL OF CHEMISTRY

https://doi.org/10.14233/ajchem.2023.28283

Generation of Pure H_2 through CH_4 Cracking Over Ni Supported on ZrO_2 Modified Al_2O_3 Catalyst

VENKATESHWARLU KANDUKURI[1], KALPANA MANDA[2], HARI PADMASRI AYTAM[3] and CHANDRASEKHAR VASAM[1,*]

[1]Department of Pharmaceutical Chemistry, Telangana University, Nizamabad-503322, India
[2]Catalysis and Fine Chemicals Department, CSIR-Indian Institute of Chemical Technology, Tarnaka, Hyderabad-500007, India
[3]Department of Chemistry, University College of Science, Osmania University, Tarnaka, Hyderabad-500007, India

*Corresponding author: E-mail: vasamcs@yahoo.co.in; csvasam@telanganauniversity.ac.in

Received: 4 August 2023; *Accepted*: 16 August 2023; *Published online*: 28 September 2023; AJC-21400

Clean hydrogen formation *via* CH_4 cracking on a zirconia-modified alumina support at 550 ºC and atmospheric pressure with constant Ni loading. The increased H_2 yields on 20Ni/3 wt.% ZrO_2-Al_2O_3 are explained by the large Ni surface area. TEM and XRD confirmed the deactivated catalyst's graphitic origin, while Raman spectroscopy helped distinguish between ordered and disordered carbon. As determined by H_2 pulse chemisorption, the high H_2 yields produced by 20wt%Ni/3 wt.%ZrO_2-Al_2O_3 catalyst is typified by well-dispersed Ni particles and large Ni metal area.

Keywords: Hydrogen production, CH_4 decomposition, Ni Catalyst.

INTRODUCTION

The need for COx-free hydrogen is rising for automotive and industrial uses, necessitating the development of new technologies to take the place of the outdated partial oxidation of hydrocarbons and steam reforming processes now used to produce hydrogen. In order to attain appropriate H_2 purity levels for polymer electrolyte membrane (PEM) fuel cells and other industrial uses, these well-developed technologies generate hydrogen polluted with COx [1]. This necessitates a more involved separation process. Since hydrocarbons are anticipated to continue to be the primary source of hydrogen in the short-to medium-term, catalytic cracking of hydrocarbons has recently attracted more attention as a COx-free hydrogen production method [2-5]. Recent commercial uses of carbon filaments, the sole byproduct of the cracking process and the hydrocarbon with the largest proportion of hydrogen to carbon among hydrocarbons, have increased interest in methane, which has already attracted attention for other reasons [6-8].

Since carbon is deposited on the catalyst during catalytic cracking of methane, catalyst deactivation is the main issue that has been reported. Carbon either diffuses through nickel to produce carbon filaments or encloses the active sites to prevent methane from accessing them [9-11]. For the catalyst to be used again in a continuous process, the deactivated catalyst must be regenerated [12]. The constant addition of regenerated catalyst and removal of deactivated catalyst are required to carry out methane cracking in a continuous mode of operation [2,7,10]. Studies on catalyst performance and analyses of the impact of process factors have been carried out.

Nickel has been the most often utilized catalyst for methane cracking. For this study, nickel has either been supported on Al_2O_3, SiO_2 and La_2O_3 or supported and promoted with a different metal, such as Ni/Cu/Al_2O_3 [13-15], Ni/Ca/Al_2O_3 [16] and Ni/Rh/La_2O_3 [17]. Supports such as zeolites are usually employed due to their microporous nature [18]. Along with carbon black, activated carbon has also been employed as catalyst [19,20]. Cobalt has been evaluated as Co/Mo/Al_2O_3, Co/Al_2O_3 and Co/Al_2O_3/SiO_2 [13,16,21]. Investigations into other metals, like Cu and Fe, have also been conducted [22-24]. Due to the deposited carbon's ability to diffuse through the active metal site and then precipitate on the other side of the metal particle to form a carbon filament, metallic catalysts differ from carbon-based catalysts in their capacity to sustain the cracking reaction for a longer period after carbon deposition starts. The metallic active site is kept at the tip of the carbon filament by a process that keeps it exposed to reactive gases until deactivation by encasing carbon eventually. Nickel is well-

known for its strong catalytic activity, higher permitted carbon loading and affordable price for hydrocarbon cracking [25-28]. Using Ni/Cu/Al_2O_3 and Co/Mo/Al_2O_3, Qian *et al.* [13] investigated the impact of catalyst reduction on methane cracking in a fluidized bed. According to their findings, the nickel catalyst outperformed the cobalt catalyst in terms of conversion. Murata *et al.* [16] investigated the methane cracking activity of several catalysts supported on alumina. The catalysts' activities were performed in the following order: Ni/Ca/Al_2O_3 > Ni/Al_2O_3 > Co/Al_2O_3 > Fe/Al_2O_3.

Additionally, the performance and stability of the catalyst are clearly impacted by the support [14,29]. According to various studies on fixed bed reactors, the catalyst material, the kind of support, the textural characteristics of catalyst and the operating parameters are the variables that govern methane conversion and the type of carbon deposition on the catalyst [30-32]. This study examined the impact of the support type and the catalyst textural features on the rate of methane cracking in a fixed bed using nickel supported on varied loadings of ZrO_2 over Al_2O_3. BET-SA (Brunauer Emmet Teller-surface area), XRD (X-ray diffraction), H_2-TPR (H_2-temperature programmed reduction), H_2-pulse chemisorption, Raman spectroscopy and CHNS (carbon, hydrogen, nitrogen and sulphur) analysis were used to characterize the catalysts and their physico-chemical properties were correlated with the rates of H_2 production.

EXPERIMENTAL

Sudchemie-purchased g-Al_2O_3 was employed as a support and impregnated with ZrO_2 of varied loadings (1, 3, 5, 7 and 10). The ZrO_2-Al_2O_3 support is impregnated with a Ni loading optimized at 20 wt.% using Ni $(NO_3)_2 \cdot 6H_2O$ as a precursor and the cracking activity of methane was analyzed. After dissolving nickel nitrate in water by weight, the weighed support was added, and then the mixture was heated to 80 ºC. This process was repeated several times to ensure that all of the water would eventually evaporate and that nickel would be spread evenly across the support. In order to remove the water of evaporation and other impurities, the impregnated sample was dried and then calcined at 500 ºC for 5 h.

Characterization: The surface characteristics of nickel supported on ZrO_2 were assessed using N_2 adsorption at -196 ºC, employing an Autosorb 3000 physical adsorption instrument. The particular surface areas were determined using the Brunauer-Emmett-Teller (BET) method. The H_2-pulse chemisorption and H2-TPR analyses were conducted using a Microtrac BEL Corp instrument (Belcat-II, Japan). The quantification of hydrogen consumption was conducted through the analysis of effluent gas, employing a calibration curve based on the temperature-programmed reduction (TPR) of Ag_2O, following a comparable experimental procedure. The X-ray diffraction (XRD) patterns of the Al_2O_3 samples modified with ZrO_2 and Ni, in their fresh, used and reduced states, were analyzed using powder XRD analysis. The analysis was conducted using a Rigaku Miniflex X-ray diffractometer, with Ni filtered Cu$K\alpha$ radiation (λ = 0.15406 nm), in the 2θ range of 10º- 80º. The scan rate was set at 2º min^{-1} and the generator voltage and current were set at 30 kV and 15 mA, respectively. The Raman spectroscopy technique was employed with a Horriba Raman spectrophotometer. The SEM images were acquired using the JSM-7601F scanning electron microscope manufactured by JEOL, Thermofischer, while high-resolution TEM micrographs were obtained using the TALOS-F 200X transmission electron microscope manufactured by FEI.

CH_4 cracking studies: A fixed bed reactor built of quartz was loaded with about 0.05-0.1g of calcined Ni/ZrO_2-Al_2O_3 catalyst. Catalyst was reduced using a mixer of 5% H_2 balance at 550 ºC for 3 h prior to the start of the reaction. After that 30 mL/min of CH_4 was allowed to flow over the catalyst in place of 5% H_2/Ar gas at the same temperature [33]. N_2 was used as the carrier gas while a Shimadzu GC (gas chromatography) set up with a carboxen column and a TCD (thermal conductivity detector) was used to investigate the product stream from the reactor exit in real time. The analysis was performed utilizing a six-port auto-sampling valve at every 15 min regular time intervals. The reaction was continued until the concentration of methane remained constant and hydrogen gas in the GC was at a minimum. The hydrogen yields measured from both CH_4 conversion and H_2 production were cross-checked and the accumulated carbon (obtained from the recovered catalyst) was examined by CHNS. Nevertheless, the absence of substances like CO and/or CO_2 during the process confirms the mass balance. It is improbable that the CO_x species were seen when CH_4 was in contact with a decreased Ni surface [34].

RESULTS AND DISCUSSION

N_2 physisorption studies: At liquid nitrogen temperature and different pressures, the nitrogen is physiosorbed on the catalyst surface and the results are tabulated in Table-1. An observed correlation exists between the elevated proportion of ZrO_2 loading and a reduction in the surface area of catalyst. This phenomenon can perhaps be attributed to the obstruction of the alumina support's pores. The surface area of the alumina

TABLE-1
PHYSICO-CHEMICAL CHARACTERISTICS OF 20 wt.% Ni SUPPORTED on ZrO_2-Al_2O_3

ZrO_2 (wt.%) in Ni/ZrO_2-Al_2O_3	BET-SA (m^2/g)[a]	Crystallite size (NiO)[b]	H_2 uptake (mmol/g)[c]	H_2 uptake (cm^3/g)[d]	Ni metal surface area (m^2/g)[e]	H_2 Yields (molH_2/mol Ni)
0	450	–	–	–	–	–
1	245	8.5	1.54	0.05	1.23	241
3	236	16.8	2.20	0.12	2.80	476
5	218	22.3	2.30	0.09	2.20	426
7	204	26.2	2.42	0.06	2.12	205
10	187	30.1	2.39	0.05	1.99	165

[a]Calculated from BET surface area; [b]XRD analysis; [c]H_2 TPR; [d, e]H_2 pulse chemisorption.

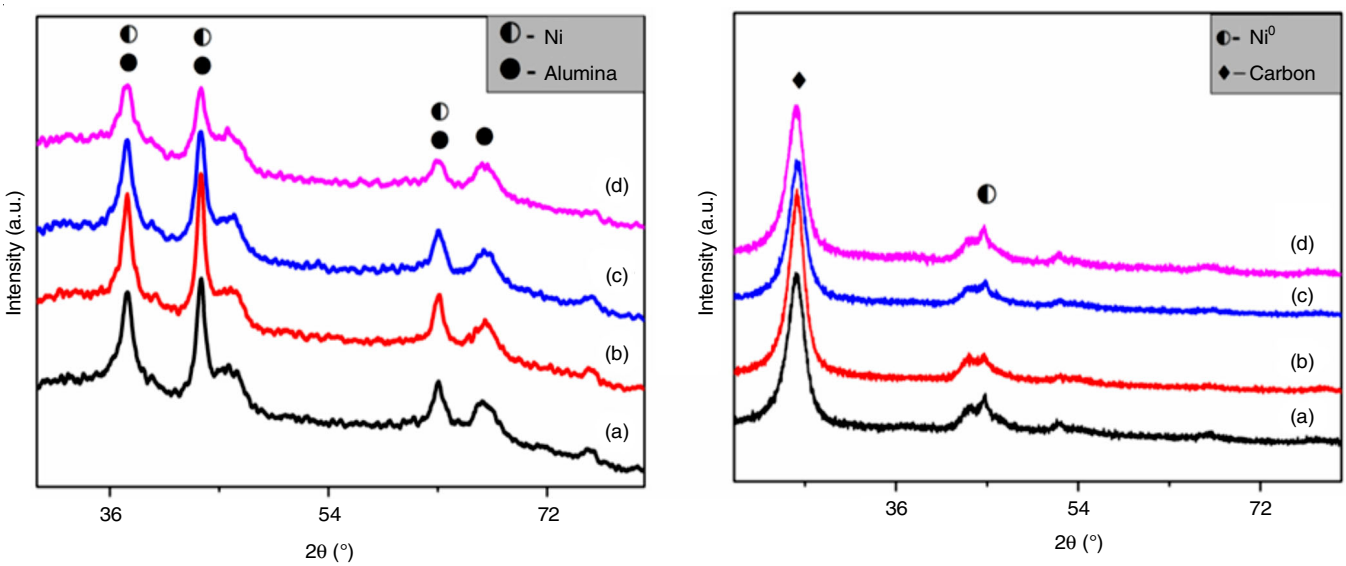

Fig. 1. XRD patterns of (A) fresh calcined and (B) used, 20 wt.% Ni over (a) 1 (b) 3 (c) 5 (d) 7 (e) 10 wt.% of ZrO_2-Al_2O_3 catalysts

which was ~ 450 m^2/g was reduced to 187 m^2/g with impregnation up to 10 wt.% of ZrO_2 and 20 wt.% of Ni.

XRD studies: Fig. 1 displays the XRD profiles of 20 wt.% Ni-X wt.%-ZrO_2-Al_2O_3 calcined at 500 ºC. The reflections at 2θ = 37.28º, 43.3º and 62.9º, along with the associated 'd' values of 2.09, 1.48 and 2.41 Å, demonstrated that NiO phase is present [ICDD #01-1239]. Since there are no reflections matched to the ZrO_2 phases, ZrO_2 is either in amorphous or micro-crystalline state beyond X-ray diffraction detection limits. Due to the well-dispersed or small crystallite size of NiO in the calcined samples, broad NiO peaks are present. Additionally, despite the constant Ni content throughout all the prepared samples, it was found that the crystallinity of NiO phase increases with an increase in ZrO_2 content, supporting the role of Al_2O_3 in promoting the crystallinity of nickel oxide phase. It appears that ZrO_2 is effectively distributing NiO species in the environment.

H_2-TPR studies: The H_2-TPR (Fig. 2) analysis was used to examine the reduction behaviour of the metal oxides and Table-1 lists the relevant hydrogen uptakes. Due to the NiO's single stage reduction, a strong peak was visible in all of the samples. The H_2 uptakes increased as the Ni loading increase, demonstrating H_2-TPR to be a bulk technique. With an increase in Ni loading, the T_{max} of the signal is somewhat pushed towards a lower temperature owing to the formation of larger NiO crystallites as determined by XRD analysis (Table-1). Additionally, a high temperature shoulder peak at 581 ºC was observed in 20 wt.%Ni-5 wt.%-ZrO_2-Al_2O_3, indicating a strong interaction between NiO species and the support. The XRD examination of 5 wt.% ZrO_2 modified catalyst provided additional support for this, revealing a shift in the diffraction angle towards a lower value (Fig. 1a). Though all the samples showed more or less similar reduction temperature, the H_2 uptake clearly manifests the effect of particle size of the catalysts or particle agglomeration during catalyst preparation. Though 20Ni-1 wt.% ZrO_2-Al_2O_3 showed high surface area the low H_2 uptake obtained on Ni surface may be due to particle agglomeration.

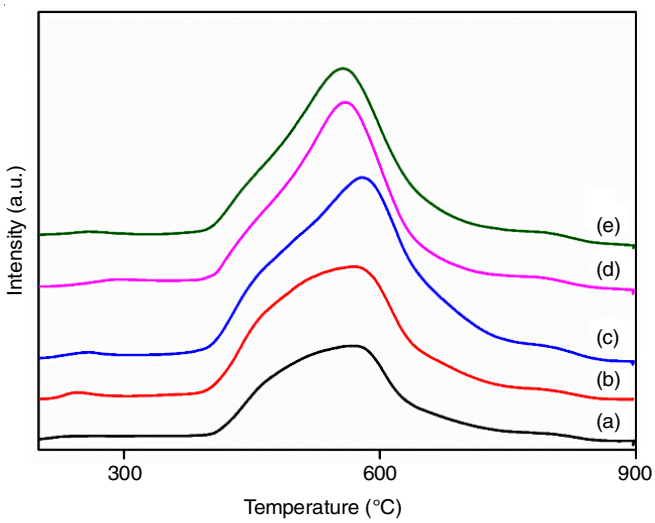

Fig. 2. H_2 TPR patterns of 20 wt.% Ni over (a) 1 (b) 3 (c) 5 (d) 7 and (e) 10 wt.% ZrO_2-Al_2O_3 catalysts

H_2 chemisorption studies: The Ni metal surface area of the samples was calculated using H_2 pulse chemisorption technique. According to the H_2 chemisorption data (Table-1), the Ni metal surface area increased from 1.23 to 2.08 $m^2\ g^{-1}$ after which it remained largely unchanged. As seen by the higher T_{max} for 5 wt.% ZrO_2 modified alumina support (Fig. 2), the low temperature reduction of 20 wt.% Ni-3 wt.% ZrO_2-Al_2O_3 catalyst appears to improve the dispersion of nickel species on the catalytic surface.

Cracking activity of methane: The time on stream (TOS) measurement of CCM activity carried out at 550 ºC with 20 wt.% Ni supported on X%-ZrO_2-Al_2O_3 catalysts is shown in Fig. 3 and the H_2 yields obtained are provided in Table-1. The activity data clearly demonstrates a higher CH_4 cracking conversion at the beginning followed by a decline with time that lasted for around 420 min. The catalytic cracking of methane (CCM) conversion was minimal and the catalyst deactivated after 300 min with decreased ZrO_2 content. Amongst these catalysts,

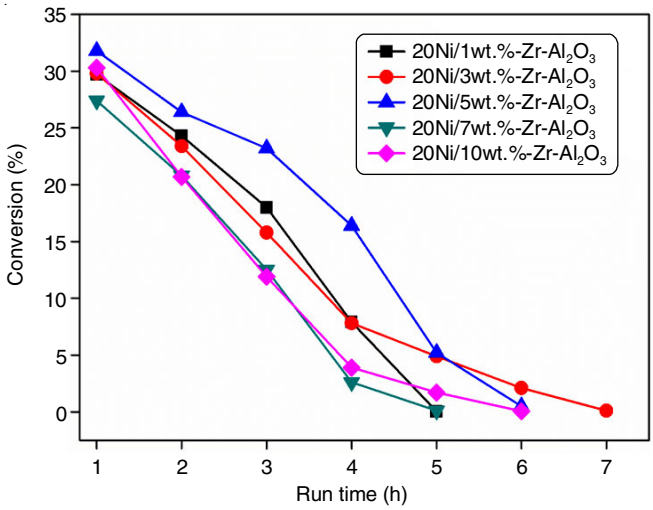

Fig. 3. TOS graph of 20Ni/X%-ZrO_2-Al_2O_3

20Ni/3 wt.% ZrO_2-Al_2O_3 showed a greater activity, which stands correlated with the hydrogen yields and the Ni metal surface area as shown in Table-1.

SEM/TEM studies: The microscopic images of the calcined catalyst showed the even distribution of the metal on the support while the used catalyst had CNT with Ni at the tip. SEM images showed the CNT ranging from 50 to 120 nm (Fig. 4a-b). The growth of the CNT obtained varies depending upon the Ni particle size [35]. Transmission electron micrograph (Fig. 4c) showed the interior of the catalyst with selvedge behaviour of the carbon and diffusion in the 'V' shape.

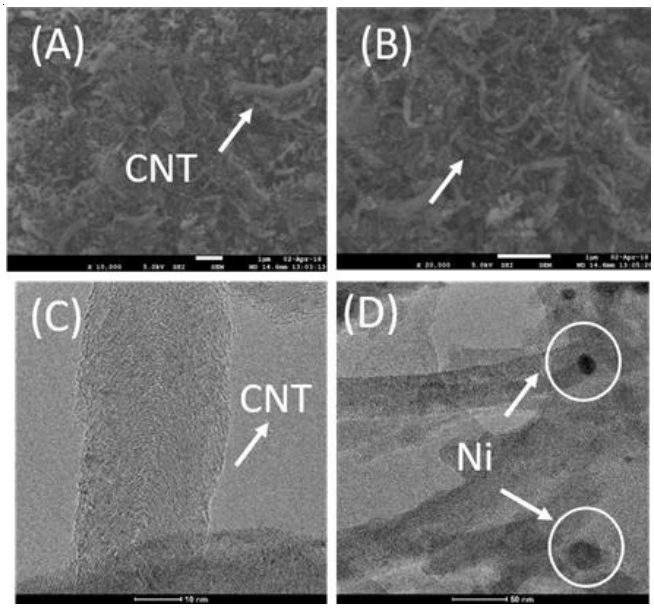

Fig. 4. SEM & TEM images of used 20Ni/3wt.%-ZrO_2-Al_2O_3

Raman spectroscopic studies: Raman spectra of the modified 20Ni/X%-ZrO_2-Al_2O_3 catalyst, which are reported in Fig. 5, confirm the type of deposition of carbon. Two different bands are observed in the Raman spectra. The one centred ~ 1320 cm^{-1} (D-band) can be attributed to disordered carbon caused by structural flaws in graphite or the presence of amorphous and carbon nanoparticles. The in-plane carbon-carbon stretching vibrations from carbon with a rather ordered structure are responsible for the Raman shift at about 1580 cm^{-1} (G-band) [31,36]. The frequency and strength of the Raman D and G bands can be used to determine the degree of crystallinity of carbon that has been deposited. The average plane size of the perfect graphene is inversely related to the ratio of the peak area of the D band to that of the G band I_D/I_G, which means that the degree of graphitization of carbons is higher at lower I_D/I_G values [37]. It has been observed that the I_D/I_G ratio fell as FWHM increased. Alvarez *et al.* [38] found a similar relationship between the I_D/I_G ratio and the FWHM for carbon nanofibers. The generation of highly ordered carbon over 20Ni/3 wt.%-ZrO_2-Al_2O_3, where the I_D/I_G ratio is smaller than other catalysts, is suggested by the carbon built-up against the G-bandwidth. The 20Ni/3 wt.%-ZrO_2-Al_2O_3 catalyst's high catalytic decomposition of methane (CDM) activity may be related to the high amount of ordered carbon that was deposited there, which eventually accumulated more carbon and persisted for a longer period than on the other catalysts. When compared to the other samples, high Ni metal surface area of 20Ni/3 wt.%-ZrO_2-Al_2O_3 may also be responsible for its CDM activity.

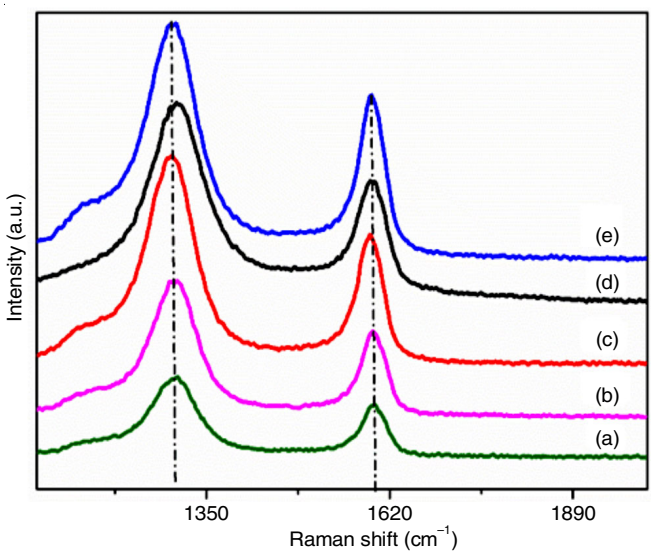

Fig. 5. Raman spectra of 20 wt.% Ni over (a) 1 (b) 3 (c) 5 (d) 7 and (e) 10 wt.% ZrO_2-Al_2O_3 catalyst

Methane cracking over alumina support has been reported by Amin *et al*. [39]. Zirconia acts as a promoter and helps in reforming of CH_4 with La_2O_3 as a support material [40]. Herein, we reported a mesoporous support such as alumina with different loadings of ZrO_2 and a constant optimized loading of Ni. The results were interesting, though the weight percent of Ni was kept constant, there occurred a decrease in surface areas of the catalysts with different contents of ZrO_2 in it. Mahesh *et al.* [41] reported the effect of promoter on the catalyst irrespective of the metallic or active component in it. The decrease in surface area of alumina support allowed for easy dispersion of the metal up to 3 wt.% and there after caused the agglomeration of the Ni which was evident from the H_2-TPR results (Fig. 2). The high metallic surface area as obtained by H_2 chemisorption also shows the effect of increased loading on the

dispersion as there was a downfall of the surface area with increase in the ZrO_2 loading above 3 wt.%. The better activity of the catalyst depends on the availability of the active component [42].

The presence of Ni as NiO in calcined sample and the Ni^0 in the reduced catalyst as observed by XRD data shows the involvement of metallic Ni for CH_4 activity. At 550 ºC and atmospheric pressure 20Ni/3 wt.% ZrO_2-Al_2O_3, showed high H_2 yields of 476 mol H_2/mol Ni while 10 wt.% ZrO_2 showed low yields of H_2 (165 mol H_2/mol Ni). The better activity of 20 wt.%Ni/3 wt.% ZrO_2-Al_2O_3 catalyst can be explained by the high dispersion of Ni as evident from H_2 chemisorption data (Table-1). The used or spent catalyst showed a high degree of graphitization with the best catalyst and low I_D/I_G ratio. The carbon in the form of CNT is deposited over the catalyst and recovered after reaction. The increase in the weight of the used catalyst is another indication of better activity of the catalyst (20Ni/3 wt.% ZrO_2-Al_2O_3). When observed by microscopic techniques, it was observed that carbon was in the form of long tubes with Ni being at the tip. As the morphology suggests that the mechanism of the CNT formation is tip growth (Fig. 4).

Conclusion

In conclusion, the catalytic cracking of CH_4 was carried out on an Al_2O_3 support modified with ZrO_2, with a constant Ni loading. The Ni metal surface of ZrO_2 modified Al_2O_3 determines hydrogen yields. Compared to other catalysts, the 20Ni/3 wt.% ZrO_2-Al_2O_3 showed better methane cracking activity. The XRD and TEM analyses of deactivated catalysts indicated the filamentous carbon formed to exhibit graphitic character. The similarity in size between the Ni particle and the carbon nanofiber was observed. Raman and XRD spectra of the deactivated catalysts were used to identify the characteristics of ordered and disordered carbons. The findings of the H_2 pulse chemisorption showed that high Ni metal surface area on 20Ni/3 wt.% ZrO_2-Al_2O_3 showed higher hydrogen yields, which is explained by the type of carbon that was deposited. The greater hydrogen yields eventually obtained by 20Ni/3 wt.% ZrO_2-Al_2O_3 are characterized by well-dispersed Ni particles, a high Ni metal surface area and a build-up of well-ordered carbon.

ACKNOWLEDGEMENTS

The authors thank the TSCOST-India for the financial support (Lr. No. 03/TSCOST/DST-PRG/2021-22, Dated: 21-03-2022), Telangana University and Osmania University for the research facilities.

CONFLICT OF INTEREST

The authors declare that there is no conflict of interests regarding the publication of this article.

REFERENCES

1. B.C. Tashie-Lewis and S.G. Nnabuife, *Chem. Eng. J. Adv.*, **8**, 100172 (2021); https://doi.org/10.1016/j.ceja.2021.100172
2. H.F. Abbas and W.M.A. Wan Daud, *Int. J. Hydrogen Energy*, **35**, 1160 (2010); https://doi.org/10.1016/j.ijhydene.2009.11.036
3. N. Muradov and T. Vezirolu, *Int. J. Hydrogen Energy*, **30**, 225 (2005); https://doi.org/10.1016/j.ijhydene.2004.03.033
4. N.Z. Muradov and T.N. Veziroglu, *Int. J. Hydrogen Energy*, **33**, 6804 (2008); https://doi.org/10.1016/j.ijhydene.2008.08.054
5. P. Ammendola, R. Chirone, G. Ruoppolo, G. Russo and R. Solimene, *Int. J. Hydrogen Energy*, **33**, 2679 (2008); https://doi.org/10.1016/j.ijhydene.2008.03.033
6. I. Suelves, M.J. La'zaro, R. Moliner, B.M. Corbella and J.M. Palacios, *Int. J. Hydrogen Energy*, **30**, 1555 (2005); https://doi.org/10.1016/j.ijhydene.2004.10.006
7. N.Z. Muradov, *Int. J. Hydrogen Energy*, **18**, 211 (1993); https://doi.org/10.1016/0360-3199(93)90021-2
8. A. Amin, E. Croiset and W. Epling, *Int. J. Hydrogen Energy*, **36**, 2904 (2011); https://doi.org/10.1016/j.ijhydene.2010.11.035
9. J.I. Villacampa, C. Royo, E. Romeo, J.A. Montoya, P. Del Angel and A. Monzo'n, *Appl. Catal. A Gen.*, **252**, 363 (2003); https://doi.org/10.1016/S0926-860X(03)00492-7
10. M. Rahman, E. Croiset and R. Hudgins, *Top. Catal.*, **37**, 137 (2006); https://doi.org/10.1007/s11244-006-0015-8
11. J. Guo, H. Lou and X. Zheng, *Carbon*, **45**, 1314 (2007); https://doi.org/10.1016/j.carbon.2007.01.011
12. P. Ammendola, R. Chirone, G. Ruoppolo and G. Russo, *Exp. Therm. Fluid Sci.*, **34**, 262 (2010); https://doi.org/10.1016/j.expthermflusci.2009.10.020
13. W. Qian, T. Liu, F. Wei, Z. Wang and Y. Li, *Appl. Catal. A Gen.*, **258**, 121 (2004); https://doi.org/10.1016/j.apcata.2003.08.017
14. J.L. Pinilla, R. Moliner, I. Suelves, M.J. La'zaro, Y. Echegoyen and J.M. Palacios, *Int. J. Hydrogen Energy*, **32**, 4821 (2007); https://doi.org/10.1016/j.ijhydene.2007.08.013
15. Z. Mohamed, V.D.B.C. Dasireddy, S. Singh and H.B. Friedrich, *Appl. Catal. B*, **180**, 687 (2016); https://doi.org/10.1016/j.apcatb.2015.07.012
16. K. Murata, M. Inaba, M. Miki and T. Yamaguchi, *React. Kinet. Catal. Lett.*, **85**, 21 (2005); https://doi.org/10.1007/s11144-005-0238-x
17. M.E. Rivas, C.E. Hori, J.L.G. Fierro, M.R. Goldwasser and A. Griboval-Constant, *J. Power Sources*, **184**, 265 (2008); https://doi.org/10.1016/j.jpowsour.2008.06.002
18. M.M. Reddy, M.A. Kumar, P. Swamy, M. Naresh, K. Srujana, L. Satyanarayana, A. Venugopal and N. Narender, *Green Chem.*, **15**, 3474 (2013); https://doi.org/10.1039/c3gc41345d
19. K.K. Lee, G.Y. Han, K.J. Yoon and B.K. Lee, *Catal. Today*, **93-95**, 81 (2004); https://doi.org/10.1016/j.cattod.2004.06.080
20. S.J. Prasad, V. Dhand, V. Himabindu and Y. Anjaneyulu, *Int. J. Energy Environ.*, **1**, 607 (2010).
21. G. Italiano, A. Delia, C. Espro, G. Bonura and F. Frusteri, *Int. J. Hydrogen Energy*, **35**, 11568 (2010); https://doi.org/10.1016/j.ijhydene.2010.05.012
22. H.T. Jang and W.S. Cha, *Korean J. Chem. Eng.*, **24**, 374 (2007); https://doi.org/10.1007/s11814-007-5037-9
23. N. Shah, S. Ma, Y. Wang and G.P. Huffman, *Int. J. Hydrogen Energy*, **32**, 3315 (2007); https://doi.org/10.1016/j.ijhydene.2007.04.040
24. P. Ammendola, R. Chirone, G. Ruoppolo and G. Russo, *Combust. Sci. Technol.*, **180**, 869 (2008); https://doi.org/10.1080/00102200801894174
25. G. Bonura, O. Di Blasi, L. Spadaro, F. Arena and F. Frusteri, *Catal. Today*, **116**, 298 (2006); https://doi.org/10.1016/j.cattod.2006.05.075
26. M. Borghei, R. Karimzadeh, A. Rashidi and N. Izadi, *Int. J. Hydrogen Energy*, **35**, 9479 (2010); https://doi.org/10.1016/j.ijhydene.2010.05.072
27. M.A. Ermakova, D.Y. Ermakov and G.G. Kuvshinov, *Appl. Catal. A Gen.*, **201**, 61 (2000); https://doi.org/10.1016/S0926-860X(00)00433-6

28. M.A. Ermakova and D.Y. Ermakov, *Catal. Today*, **77**, 225 (2002); https://doi.org/10.1016/S0920-5861(02)00248-1
29. S. Takenaka, H. Ogihara, I. Yamanaka and K. Otsuka, *Appl. Catal. A Gen.*, **217**, 101 (2001); https://doi.org/10.1016/S0926-860X(01)00593-2
30. F.-J. Spiess, S.L. Suib, K. Irie, Y. Hayashi and H. Matsumoto, *Catal. Today*, **89**, 35 (2004); https://doi.org/10.1016/j.cattod.2003.11.043
31. Y. Li, B. Zhang, X. Xie, J. Liu, Y. Xu and W. Shen, *J. Catal.*, **238**, 412 (2006); https://doi.org/10.1016/j.jcat.2005.12.027
32. J. Ashok, S. Naveen Kumar, A. Venugopal, V. Durga Kumari and M. Subrahmanyam, *J. Power Sources*, **164**, 809 (2007); https://doi.org/10.1016/j.jpowsour.2006.11.029
33. W. Yan and S.K. Hoekman, *Environ. Prog. Sustain*, **33**, 213 (2014); https://doi.org/10.1002/ep.11746
34. K. Manasa, G. Naresh, M. Kalpana, B. Sasikumar, V.K. Velisoju, K.V.R. Chary, B. Michalkiewicz and A. Venugopal, *J. Energy Inst.*, **99**, 73 (2021); https://doi.org/10.1016/j.joei.2021.08.005
35. G. Naresh, V. Vijay Kumar, C. Anjaneyulu, J. Tardio, S.K. Bhargava, J. Patel and A. Venugopal, *Int. J. Hydrogen Energy*, **41**, 19855 (2016); https://doi.org/10.1016/j.ijhydene.2016.09.131
36. L. Dussault, J.C. Dupin, C. Guimon, M. Monthioux, N. Latorre, T. Ubieto, E. Romeo, C. Royo and A. Monzon, *J. Catal.*, **251**, 223 (2007); https://doi.org/10.1016/j.jcat.2007.06.022
37. H. Darmstadt, L. Summchen, J.M. Ting, U. Roland, S. Kaliaguine and C. Roy, *Carbon*, **35**, 1581 (1997); https://doi.org/10.1016/S0008-6223(97)00116-4
38. W.E. Alvarez, F. Pompeo, J.E. Herrera, L. Balzano and D.E. Resasco, *Chem. Mater.*, **14**, 1853 (2002); https://doi.org/10.1021/cm011613t
39. A. Amin, E. Croiset, C. Constantinou and W. Epling, *Int. J. Hydrogen Energy*, **37**, 9038 (2012); https://doi.org/10.1016/j.ijhydene.2012.02.001
40. B. Bachiller-Baeza, C. Mateos-Pedrero, M.A. Soria, A. Guerreroruiz, U. Rodemerck and I. Rodríguez-Ramos, *Appl. Catal. B*, **129**, 450 (2013); https://doi.org/10.1016/j.apcatb.2012.09.052
41. M. Dumpalapally, S. Boggala, R.C. Nappuni, S. Varimalla and V. Akula, *Chem. Eng. Sci.*, **278**, 118922 (2023); https://doi.org/10.1016/j.ces.2023.118922
42. K. Manda, M. Kandula, P.H. Aytam, P. Basak, A.V.S. Sarma and V. Akula, *Environ. Prog. Sustain.*, e14222 (2023); https://doi.org/10.1002/ep.14222